



## FULL PAPER

# Water Soluble Nickel – metformin ternary complexes: Thermal, DNA binding and molecular docking studies

K. Rajeshwari<sup>1</sup> | P. Vasantha<sup>1</sup> | B.S. Kumar<sup>2</sup> | B. Shekhar<sup>2</sup> | P.V.A. Lakshmi<sup>2</sup>

<sup>1</sup>Department of Chemistry, University College for Women, Osmania University, Koti, Hyderabad, Telangana State, 500095, India

<sup>2</sup>Department of Chemistry, Osmania University, Tarnaka, Hyderabad, Telangana State, 500007, India

**Correspondence**

Anantha Lakshmi, Department of Chemistry, Osmania University, Tarnaka, Hyderabad, Telangana State, 500007, India.

Email: pvanantha.ou@gmail.com

**Funding information**

Department of Science and Technology, Ministry of Science and Technology, Grant/Award Number: PURSE II

The Nickel (II) complexes [Ni(Cl)<sub>2</sub>(metf)(o-phen)] (**1**), [Ni(Cl)<sub>2</sub>(metf)(opda)] (**2**), [Ni(Cl)<sub>2</sub>(metf)(en)] (**3**), [Ni(Cl)<sub>2</sub>(metf)(2,2'-bipy)] (**4**), (metf = metformin, o-phen = ortho-phenanthroline, opda = ortho-phenylenediamine, en = ethylenediamine, 2-2' bipy = 2-2' bipyridyl) were synthesized and characterized using LC-MS, elemental analysis, molar conductance measurements, TGA-DTA, IR spectroscopy, magnetic moment measurements and electronic spectroscopy. The central Ni<sup>2+</sup> was found to be in octahedral geometry. The DNA interaction of these complexes have been studied by UV-visible absorption studies, fluorescence emission technique and viscosity measurement. The complexes showed absorption hyperchromism in UV-visible spectra with calf thymus DNA. The binding constants from UV-visible absorption studies were  $7.42 \times 10^4$ ,  $0.74 \times 10^4$ ,  $3.19 \times 10^4$ ,  $5.9 \times 10^4$  M<sup>-1</sup> for **1**, **2**, **3** and **4**, respectively and Stern-Volmer quenching constants from fluorescence studies were 0.16, 0.41, 0.23, 0.18, respectively. Viscosity measurements revealed that the binding of the complexes with DNA could be surface binding, mainly due to groove binding. The highest DNA cleavage activity of the complexes is recorded for complex **1**. The complexes were docked in to B-DNA sequence, 5'(D\*AP\*CP\*CP\*GP\*AP\*CP\* GP\*TP\*CP\*GP\*GP\*T)-3' retrieved from protein data bank (PDB ID: 423D), using Discovery Studio 2.1 software. C Docker Inttraction energy of **1**, **2**, **3** and **4** complexes is 32.027, 31.427, 35.393 and 30.521 respectively. The highest docking score is seen for complex **3**.

**KEYWORDS**

DNA, docking, groove binding, metformin, nickel complexes

## 1 | INTRODUCTION

Bioinorganic chemistry usually is the study of the interaction of inorganic elements with organisms at molecular level.<sup>[1]</sup> The interaction of biological macromolecules like DNA with transition metal complexes has become an important research topic and helps us to understand the life processes at molecular level.<sup>[2,3]</sup> Many transition metal complexes act as excellent chemotherapeutic agents and exert their biological activity like anticancer,

by binding with DNA, thereby altering DNA replication, blocking the division of cancer cells and resulting in cell death.<sup>[4]</sup> Interaction with DNA are not the only factors that determine the biological activity of these complexes, but their reactivity and selectivity are often correlated with their mode of binding with DNA. Therefore it is essential to understand the various factors that govern the interaction of small molecules with DNA. In general, drugs interact with DNA in three distinct modes of noncovalent interactions, groove binding through a

combination of hydrophobic, electrostatic, and hydrogen-bonding interactions; intercalative association in which a planar, aromatic moiety slides between the DNA base pairs; and external binding by electrostatic attraction.<sup>[5,6]</sup>

Metformin.HCl (Chemically known as N,N-dimethylbiguanide) is chosen as primary ligand because of its wide spread applications in medicinal field and its ability to chelate metal strongly. Metformin is a powerful oral antihyperglycemic drug that has been used in many countries for over 40 years for treating diabetic patients with non-insulin dependent diabetes mellitus (NIDDM).<sup>[7]</sup> Metformin acts as glucose lowering agent, analgesic, anti-malarial and anti-metabolite for organisms that inhibit the metabolism of folic acid. It is well known that these biguanide derivatives exhibit both biological and coordinative properties.<sup>[8]</sup> Recently, it was found that vanadyl complex with metformin shows potential synergistic insulin mimics,<sup>[9]</sup> while platinum (IV) complexes reveals antitumor activity.<sup>[10]</sup> The interaction of metformin with calf thymus DNA (CT-DNA) has been investigated by Shahabadi and Heidari.<sup>[11]</sup> The DNA binding studies of Pt (II) Complexes with metformin. HCl (metf) as ligand have been studied by Nahid Shahabadi et al. They have reported the interaction of Pt (II) Complex with DNA via groove binding mode.<sup>[12]</sup>

Nickel is an essential trace element for human body and the metalloenzymes containing Nickel (II) play important physiological functions in the organisms.<sup>[13]</sup> Nickel (II) complexes have been reported to act as anti-convulsant and antiepileptic agents or vitamins, they have also presented antibacterial,<sup>[14]</sup> antifungal,<sup>[15]</sup> antimicrobial,<sup>[16]</sup> antioxidant<sup>[17]</sup> and anticancer activities.<sup>[18]</sup> Therefore the research of Nickel (II) complexes has attracted more attention and become more important in the field of bioinorganic and co-ordination chemistry.<sup>[19]</sup> The interaction of Nickel (II) complexes with DNA has become an important research topic. These Nickel (II) complexes exhibit anticancer activity by binding to DNA base pairs, there by altering DNA replication, blocking the division of cancer cells and resulting in cell death. For example Nickel (II) Complexes of Benzoic acid (2-hydroxy- benzyldine)-hydrazide ligands bind to DNA base pairs via intercalation and  $\pi$ - $\pi$  stacking interactions. Nickel (II) complexes containing N-substituted heterocyclic thiosemicarbazones have been found to exhibit remarkable DNA/protein binding and antioxidant activities.<sup>[20]</sup> In addition Nickel (II) complexes have attracted the attention of researchers because of their superoxide scavenger activities and broad biological activities.<sup>[21]</sup>

A literature survey reveals that Nickel complexes have various DNA binding properties and biological properties. So, we planned the synthesis of complexes using Nickel metal ion. In spite of its widespread

application, metformin and its ternary complexes have received less attention. Hence, it is focused to synthesize, characterize and study DNA binding properties of Ni (II)-metformin ternary complexes.

The aim of this paper is to report the synthesis, characterization and DNA binding studies of Nickel (II)-metformin complexes containing 1,10-phenanthroline or o-phenylenediamine or ethylenediamine or 2,2'-bipyridyl as auxiliary ligand. The binding properties of the Nickel (II) complexes with CT-DNA in Tris -HCl buffer (PH = 7) were investigated by multi- spectroscopic methods. From the results of UV absorbtion spectra, viscosity and fluorescence displacement experiments, the binding mode of interaction between Ni (II) complexes and DNA were obtained.

## 2 | EXPERIMENTAL

### 2.1 | Materials and methods

All the chemicals used were either of AR grade or chemically pure grade. Metformin was procured from Emmennar Pharma Pvt Ltd. CT (Calf Thymus) DNA was purchased from Himedia (stored at  $-20^{\circ}\text{C}$ ) and was used as received. Supercoiled pUC19 plasmid DNA (stored at  $-20^{\circ}\text{C}$ ) was obtained from Fermentas Life Sciences and agarose from Genei.

For preparing various buffers, double-distilled water was used. Binding studies of the complexes with CT-DNA were conducted using Tris -HCl buffer (5 mM Tris -HCl, 50 mM NaCl; pH = 7.2). A ratio of UV absorbance of CT- DNA solution at 260 and 280 nm of 1.8–1.9 indicated that the DNA was sufficiently free of protein.<sup>[22]</sup> The DNA concentration per nucleotide was determined by absorption spectroscopy using the molar absorption coefficient ( $6600\text{ M}^{-1}\text{ cm}^{-1}$ ) at 260 nm.<sup>[23]</sup> Stock solutions were stored at  $4^{\circ}\text{C}$  and used after no more than four days. Concentrated stock solutions of metal complexes were prepared in buffer for all experiments.

### 2.2 | Instrumentation

UV-visible spectra were recorded with a Shimadzu 240A spectrophotometer. Fluorescence spectra were recorded with Shimadzu 5301 spetrofluorophotometer. Infrared (IR) spectra were recorded using KBr discs in the range  $400\text{--}4000\text{ cm}^{-1}$  with a Perkin Elmer FT-IR spectrometer. Solid-state UV-visible spectra of the complexes were recorded with a Shimadzu 160A spectrophotometer (200–800 nm). Elemental microanalysis (C, H and N) was carried out with a Perkin Elmer 240 elemental analyser.

Chloride analysis was carried out using Mohr's method. The metal contents were estimated using a Shimadzu AA-6300 atomic absorption spectrophotometer. Mass spectra were recorded with a Shimadzu LCMS-2010 A spectrometer. Molar conductance was measured using an Elico Digital conductivity bridge (model CM-180) with a dip-type cell. Magnetic susceptibilities were recorded at room temperature with a Faraday magnetic susceptibility mill balance (model 7550), using  $\text{Hg}[\text{Co}(\text{NCS})_4]$  as the standard. Diamagnetic corrections were made using Pascal's constants.<sup>[24]</sup> Thermal analysis was carried out using a TGA Q 5000 V3.13 build 261 instrument.

### 2.3 | Synthesis of metal complexes

Metformin (0.166 g, 1 mmol) was dissolved in 5 ml of 0.1 N KOH solution.  $\text{NiCl}_2 \cdot 6\text{H}_2\text{O}$  (0.238 g, 1 mmol) in 5 ml of water was added to the metformin solution, in the presence of 1,10-phenanthroline (0.198 g, 1 mmol) or o-phenylenediamine (0.108 g, 1 mmol) or ethylenediamine (0.133 g, 1 mmol) or 2,2'-bipyridyl (0.156 g, 1 mmol) at room temperature. The reaction mixture was heated for 1 hr using a water bath and the complexes that separated out were filtered and dried. The purity of the complexes was determined by TLC using various solvent mixtures. The melting points of the complexes were above 300 °C.

### 2.4 | DNA binding studies

Absorption titration experiments were performed by maintaining a constant metal complex concentration (20  $\mu\text{M}$ ) and varying the DNA concentration (0–100  $\mu\text{M}$ ) in the buffer. After each addition of DNA to the metal complex, the resulting solution was allowed to equilibrate at 25 °C for 5 min, after which the change in absorption intensity of the ligand to metal charge transfer (LMCT) band was recorded. The intrinsic binding constant,  $K_b$ , was determined from the spectral data using the Wolfe-Shimmer equation:<sup>[25]</sup>  $[\text{DNA}/(\epsilon_a - \epsilon_f) = [\text{DNA}]/(\epsilon_b - \epsilon_f) + 1/K_b(\epsilon_b - \epsilon_f)]$ , where  $[\text{DNA}]$  is the concentration of the DNA in base pairs,  $\epsilon_a$  the apparent extinction coefficient ( $= A_{\text{obsd}}/[\text{complex}]$ ),  $\epsilon_f$  the extinction coefficient for free metal complex and  $\epsilon_b$  the extinction coefficient for free metal complex in fully bound form. From plots of  $[\text{DNA}]/(\epsilon_a - \epsilon_f)$  versus  $[\text{DNA}]$ , gave a slope of  $1/(\epsilon_b - \epsilon_f)$  and Y-intercept equal to  $1/K_b(\epsilon_b - \epsilon_f)$ ;  $K_b$  is given by the ratio of slope to intercept.

Fluorescence quenching experiments were carried out in 5 mM Tris-HCl/50 mM NaCl (pH = 7.5). A solution containing DNA and ethidium bromide (EB) was

titrated with varying concentrations of the complexes. The DNA concentration was always 130  $\mu\text{M}$  DNA-phosphate. The concentrations of the complexes were in the range 0–100  $\mu\text{M}$  and EB concentration was 40  $\mu\text{M}$ . The solutions were excited at 540 nm and fluorescence emission, which corresponds to 598 nm, was recorded. The Stern-Volmer quenching constant was obtained from classical Stern-Volmer equation<sup>[26]</sup>:  $I_0/I = 1 + K \cdot r$ . ( $I_0$  and  $I$  are the fluorescence intensities in the absence and presence of complexes, respectively,  $K$  is a linear quenching constant, which depends on the concentration ratio of bound EB to DNA, and  $r$  is the concentration ratio of complex to DNA). In the plot of  $I_0/I$  Vs  $[\text{complex}]/[\text{DNA}]$ ,  $K$  is given by the ratio of slope to intercept.

Emission titration experiments were performed by maintaining a constant metal complex concentration (10  $\mu\text{M}$ ) and varying the DNA concentration (10–200  $\mu\text{M}$ ) in the buffer. After each addition of DNA to the metal complex, the resulting solution was allowed to equilibrate at 25 °C for 5 min, then excited in the intense LMCT band between 350 and 400 nm, and the emission was measured at 550–700 nm. The fraction of the ligand bound was calculated from the relation  $C_b = C_t[(F - F_0)/(F_{\text{max}} - F_0)]$ , where  $C_t$  is the total complex concentration,  $F$  is the observed fluorescence emission intensity at a given DNA concentration,  $F_0$  is the intensity in the absence of DNA and  $F_{\text{max}}$  is the intensity when the complex is fully bound to DNA. Binding constant ( $K_b$ ) was obtained from a modified Scatchard plot of  $r/C_f$  versus  $r$ , where  $r = C_b/[\text{DNA}]$  and  $C_f$  is the concentration of free complex.<sup>[27]</sup> Nonlinear least-squares fitting of the data yields  $K_b$ .

Viscosity measurements were performed with an Ostwald viscometer at room temperature. The concentration of DNA was 20  $\mu\text{M}$  and complex concentration varied from 0 to 100  $\mu\text{M}$ . The flow times were measured with a digital timer and each sample was measured three times for accuracy, and an average flow time was calculated.<sup>[28]</sup> Data were presented as  $(\eta/\eta_0)^{1/3}$  versus  $[\text{complex}]/[\text{DNA}]$ , where  $\eta$  is the viscosity of DNA in the presence of complex and  $\eta_0$  that of DNA alone. Viscosity values were calculated from the observed flow time of DNA-containing solutions ( $t$ ) corrected for buffer (5 mM Tris-HCl/50 mM NaCl) alone ( $t_0$ ):  $\eta = (t - t_0)$ .

To perform DNA Cleavage studies of the complexes pUC19DNA was used and the studies were performed by using gel electrophoresis technique. Buffer solutions used in this technique are TE buffer (1 mM  $\text{Na}_2\text{EDTA}$  and 10 mM Tris-HCl) and TAE buffer (Tris-acetate EDTA, 1 mM EDTA, Tris-base, 20 mM acetic acid) and TE and TAE buffer is maintained at pH 8.0. To prepare pUC19DNA stock solution TE buffer solution was used. pUC19 DNA (0.1  $\text{g } \mu\text{L}^{-1}$ ) was allowed to react with varying concentration of complexes (1, 2, 3 and 4) and the

volume of the solution was made to 16  $\mu\text{L}$  by using Tris-HCL buffer solution. To the above solution 1 mM  $\text{H}_2\text{O}_2$  was added and the resulting solution was incubated for 2 hr at 37  $^\circ\text{C}$ . A dye containing 3', 3'', 5', 5''- tetra bromo phenolsulfonphthalein (bromophenol blue, 0.30%), glycerol(45%), xylene cyanol (30%) and 2 mM EDTA were added to the above incubated solution in order to quench the reaction. The sample mixtures were carefully placed into wells of gel. Electrophoresis was performed for 2 hr at 100 V using 1% agarose gel in TAE (Tris acetic acid EDTA) buffer and ethidium bromide (1.0  $\mu\text{g}/\text{ml}$ ) was used to stain the gel. When the dye front reaches the end of the gel, electrophoresis was stopped and the images were photographed under UV light.

### 3 | RESULTS AND DISCUSSION

#### 3.1 | Characterization of metal complexes

All the complexes are colored and quite stable to air and moisture. The complexes are soluble in water, ethanol and dimethylsulfoxide. Characterization of the complexes using liquid chromatography-mass spectrometry (LC-MS), elemental analysis, molar conductance measurements, thermal analysis, IR spectroscopy, magnetic measurements, electronic spectroscopy, and geometrical studies confirm the coordination mode of the ligands.

The LC-MS spectra recorded at room temperature resolve  $M + 1$  peaks at  $m/z$  439, 319 and 415 for complexes **1**, **3**, **4** respectively and  $M - 1$  peak at  $m/z$  365 for complex **2**. Analysis of carbon, hydrogen, nitrogen, chloride and Nickel reveals the formulae  $\text{NiC}_{16}\text{H}_{19}\text{N}_7\text{C}_{12}$ ,  $\text{NiC}_{10}\text{H}_{19}\text{N}_7\text{C}_{12}$ ,  $\text{NiC}_6\text{H}_{19}\text{N}_7\text{C}_{12}$ ,  $\text{NiC}_{14}\text{H}_{19}\text{N}_7\text{C}_{12}$  for complexes **1**, **2**, **3** and **4** respectively. The ratio of metformin, auxiliary ligand and Nickel (II) in these complexes is 1:1:1. The analytical data of prepared complexes are presented in the Table 1. The conductivity of metformin complexes was measured for aqueous solution at room temperature. The complexes show molar conductance values of 2 to 4  $\Omega^{-1}\text{cm}^2\text{mol}^{-1}$  for  $10^{-3}$  M concentration, indicating that the complexes are non-electrolytes<sup>[29]</sup> and the presence of chloride ions within the coordination sphere of the complexes.

Thermogravimetric analysis (TGA) of **1**, **2**, **3**, **4** was conducted. They are thermally decomposed in decomposition steps mainly within the range 25–1000  $^\circ\text{C}$ .<sup>[30]</sup> Complex **1** is thermally decomposed in five successive decomposition steps within the range 29–1000  $^\circ\text{C}$ . The first step (obs. = 9.82%, calc. = 9.80%) at 29–200  $^\circ\text{C}$  may be attributed to the removal of the  $\text{CN}_2\text{H}_3$  fragment. The second step at 200–300  $^\circ\text{C}$  (obs. = 18.08%, calc. = 18.12%)

**TABLE 1** Analytical data and Physical Properties of complexes

Complex	Mol. wt.	Color	M.pt. ( $^\circ\text{C}$ )	Yield (%)	Elements found % (Calc.)					$\Lambda_m(\Omega^{-1}\text{cm}^2\text{mol}^{-1})$
					Ni	C	H	N	Cl	
1	438.71	Green	322	85	13.56 (13.37)	43.18 (43.70)	4.29 (4.33)	22.12 (22.33)	16.30 (16.18)	4.0
2	366.83	Black	348	90	15.76 (15.99)	32.38 (32.71)	5.94 (5.17)	26.23 (26.71)	19.85 (19.35)	2.5
3	318.69	Light yellow	317	80	18.73 (18.41)	22.44 (22.59)	5.41 (5.96)	30.95 (30.75)	22.45 (22.27)	4.5
4	414.88	Light green	335	92	14.53 (14.14)	40.15 (40.49)	4.84 (4.57)	23.21 (23.62)	17.55 (17.11)	3.6

is accounted for the removal of  $C_2H_6N$  and chloride ion. The third step at 300–500 °C (obs. = 24.35%, calc. = 23.47%) is accounted for the removal of  $C_7NH_5$  fragment. The fourth step at 500–700 °C (obs. = 12.93%, calc. = 11.62%) is accounted for the removal of  $C_4H_3$  fragment. The fifth step at 700–1000 °C (obs. = 7.80%, calc. = 8.09%) is attributed to the removal of chloride ion. The decomposition ends with a  $C_2H_2N_3$  and Ni ion residue (obs. = 27%, calc. = 28.88%). The TGA curve of complex **2** indicates that the mass change begins at 36 °C and continues up to 1000 °C. It is thermally decomposed in mainly five decomposition steps. The first step occurs in the range 36–100 °C and corresponds to the liberation of  $NH_2$  (obs. = 3.98%, calc. = 4.36%). The second step at 100–200 °C (obs. = 6.32%, calc. = 7.36%) is accounted for the removal of the CNH fragments. The third step (obs. = 28.551%, calc. = 29.44%) at 200–300 °C may be attributed to the liberation of the opda. The fourth decomposition step of the complex occurs in the range 300–400 °C and corresponds to the loss of 2Cl fragments (obs. = 18.84%, calc. = 19.35%). The fifth step (obs. = 23.07%, calc. = 19.35%) at 400–1000 °C and corresponds to the loss of  $C_3H_7N_2$  fragment. This fragmentation ends with a final residue of Ni-NH fragment (obs. = 19.23%, calc. = 20.09%). The TGA curve of complex **3** indicates that the mass change begins at 37 °C and continues up to 1000 °C. The complex is thermally decomposed in mainly five decomposition steps. The first step occurs in the range 37–200 °C and corresponds to the loss of C-NH<sub>2</sub> fragment. (obs. = 8.48%, calc. = 8.70%). The second step at 200–300 °C (obs. = 26.04%, calc. = 26.98%) is accounted for the removal of ( $C_3N_3H_8$ ) fragment. The third step (obs. = 21.83%, calc. = 22.27%) at 300–400 °C may be attributed to the loss of the 2Cl fragments. The fourth step occurs in the range 400–600 °C and corresponds to the loss of ( $C_2NH_6$ ) fragment (obs. = 16.256%, calc. = 13.80%). The fifth step occurs in the range 600–1000 °C and is accounted for the removal of NH and  $NH_2$  (obs. = 10.16%, calc. = 9.73%). This fragmentation ends with a final residue of Nickel metal (obs. = 17.22%, calc. = 18.42%). The TGA curve of Complex **4** indicates that the mass change begins at 36 °C and continues up to 1000 °C. It is thermally decomposed mainly in six decomposition steps. The first step occurs in the range 36–200 °C and corresponds to the loss of (C-H) fragment (obs. = 2.72%, calc. = 3.13%). The second step at 200–300 °C (obs. = 9.32%, calc. = 8.55%) is accounted for the removal of the Cl fragment. The third step (obs. = 8.3%, calc. = 8.55%) at 300–400 °C may be attributed to the loss of Cl fragment. The fourth decomposition step of the complex occurs in the range 400–500 °C and corresponds to the loss of  $C_2NH_6$  (obs. = 10.42%, calc. = 10.60%). The fifth step at 500–600 °C

(obs. = 3.94%, calc. = 3.61%) is accounted for the removal of NH fragment. The final step of decomposition of the complex at 600–1000 °C is attributed to the liberation of  $NH_2$ . This decomposition ends with a final residue of  $C_{11}H_9N_4$  and Nickel ion (obs. = 61.30%, calc. = 61.63%).

The IR Spectra of **1**, **2**, **3** and **4** were analyzed in comparison of their free ligand spectra.<sup>[31]</sup> The characteristic IR spectral bands assigned to the stretching frequencies of amine and imine groups of metformin are shifted in the spectra of all three complexes when compared with free metformin.<sup>[32]</sup> The shifting of imine band C=N of metformin at 1568  $cm^{-1}$  to 1583, 1571, 1558, and 1591  $cm^{-1}$  for complexes **1**, **2**, **3**, and **4** respectively, indicates that coordination takes place through the imine nitrogen.<sup>[33]</sup> A six-membered ring possibly also exists from coordination involving amino nitrogens; however, M–N (imino) bond formation takes priority over M–N (amino) bond formation possibly due to  $\pi$  conjugation of the C–N–C system involving the imino nitrogen.<sup>[33]</sup> The new band at around 1340, 1342, 1315 and 1311  $cm^{-1}$  in the spectra of **1**, **2**, **3**, and **4** respectively, could be associated with the chelate ring formation for the metformin complexes.<sup>[34]</sup> The shifting of the  $NH_2$ (as), NH and  $NH_2$ (s) bands of metformin at 3371, 3294 and 3172  $cm^{-1}$  to 3369, 3298, 3176; 3369, 3271, 3199; 3362, 3290, 3167  $cm^{-1}$ ; and 3365, 3298, 3172  $cm^{-1}$  for **1**, **2**, **3** and **4** respectively, indicates the coordination of metformin to metal. In the spectrum of **1**, the peaks corresponding to the ring stretching frequencies  $\nu(C=C)$  and  $\nu(C=N)$  of o-phen at 1505 and 1421  $cm^{-1}$  are shifted to higher frequencies (ca 1514 and 1479  $cm^{-1}$ ), indicating the coordination of the heterocyclic nitrogen atoms to the metal ion. The characteristic out-of-plane hydrogen-bonding modes of free o-phen observed at 853 and 738  $cm^{-1}$  are shifted to 850 and 727  $cm^{-1}$ , respectively, upon complexation.<sup>[35]</sup> The shifting of the  $\nu(NH_2)$  band of free opda at 3386 to 3309  $cm^{-1}$  for complex **2** indicates the coordination of opda to Nickel (II) through  $NH_2$  groups.<sup>[36]</sup> The  $\nu(CN)$  band at 1060  $cm^{-1}$  of free **en** is shifted to 1035  $cm^{-1}$  for **3**. The stretching frequencies of the chelate **en** are observed in the region 1500–1700  $cm^{-1}$  for  $NH_2$  bending and in the region 850–950  $cm^{-1}$  for rocking. In the spectrum of **3**,  $NH_2$  bending is observed at 1678  $cm^{-1}$  and  $CH_2$  rocking at 933  $cm^{-1}$ .<sup>[37]</sup> In the spectrum of **4**, the peaks corresponding to ring stretching frequencies of  $\nu(C=N)$ ,  $\nu(C-H)$  and  $\nu(C=C)$  of bipyridyl at 1600  $cm^{-1}$ , 3050  $cm^{-1}$  and 1450  $cm^{-1}$  are shifted to 1558  $cm^{-1}$ , 3070  $cm^{-1}$  and 1446  $cm^{-1}$ .<sup>[38]</sup> The  $\nu(Ni-N)$  band of bipyridyl complexes is observed in the range of 180–290  $cm^{-1}$ . In the spectrum of **4** this band is observed at 277  $cm^{-1}$ . The low frequency region of the spectra of all complexes reveals the presence of medium intensity

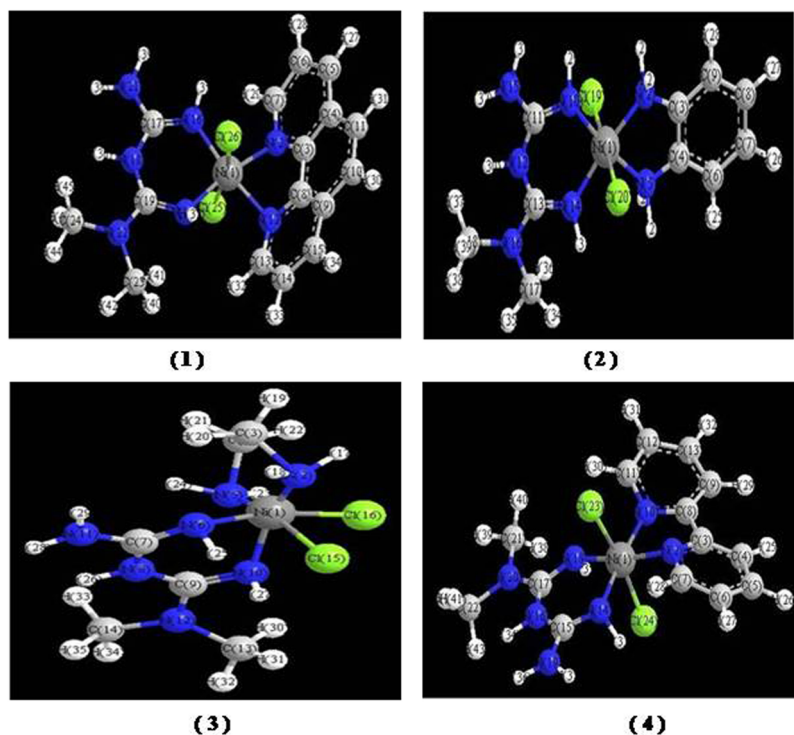
bands in the region 300–600  $\text{cm}^{-1}$  due to  $\nu(\text{M-N})$  and also  $\nu(\text{M-Cl})$  vibrations.<sup>[39]</sup> Thus, the IR data suggest that metformin and the auxiliary ligands are bound to the metal ion through nitrogen donor atoms.

Complexes **1**, **2**, **3**, and **4** show magnetic moments of 2.8, 2.7, 2.9 and 2.7 BM respectively, which are in good agreement with the presence of 2 unpaired electrons. The electronic spectra of all metal complexes were recorded. Electronic absorption spectroscopy is very useful in the evaluation of the results furnished by other methods of structure investigation. The electronic spectral measurements were used for assigning the stereochemistry of metal ions in the complexes based on the position and number of d-d transition bands. The electronic spectra of complexes **1**, **2**, **3** and **4** show bands at 8319, 17543, 22270; 8620, 12722, 22222; 11587, 18939, 23201 and 8389, 14513, 20449  $\text{cm}^{-1}$  respectively corresponding to the transitions  ${}^3\text{A}_{2g}(\text{F}) \rightarrow {}^3\text{T}_{2g}(\text{F})$  ( $\nu_1$ ),  ${}^3\text{A}_{2g}(\text{F}) \rightarrow {}^3\text{T}_{1g}(\text{F})$  ( $\nu_2$ ) and  ${}^3\text{A}_{2g}(\text{F}) \rightarrow {}^3\text{T}_{1g}(\text{P})$  ( $\nu_3$ )<sup>[40,41]</sup> which are characteristic of six-coordinate octahedral geometry of Nickel (II) complexes. A moderately intense band, seen at 29411, 29069, 28653, 27173  $\text{cm}^{-1}$  for **1**, **2**, **3** and **4**, respectively, can be assigned to ligand-to-metal charge transfer transition. The structure is also further confirmed by the ratio of  $\nu_2/\nu_1 = 2.10, 1.50, 1.63$  and  $1.73$  for **1**, **2**, **3** and **4**, respectively, which are close to the value expected for octahedral structure.<sup>[42,43]</sup> The ligand field parameters,  $10Dq$  and  $B$ , have been calculated for all four complexes.

The Racah inter-electron repulsion parameter  $B$  observed for these complexes is less than that for the free ion. The nephelauxetic parameter  $\beta = B/B'$  is less than one for these complexes.<sup>[44]</sup> All these observations suggest that the metal-ligand bond in the complexes is covalent in nature.

### 3.2 | Geometrical structure of metal complexes

Geometrical structures of complexes **1**, **2**, **3** and **4** were calculated by optimizing their bond lengths, bond angles and torsional angles. The geometrical structures are presented in Figure 1. Selected geometric values (bond lengths and bond angles) of the metal complexes are presented in Table 2. Both the highest occupied molecular orbital (HOMO) and the lowest unoccupied molecular orbital (LUMO) are the main orbitals that take part in chemical stability. The HOMO represents the ability to donate an electron. The LUMO represents the electron accepting capacity. Molecular orbital structures (HOMO and LUMO) for metal complexes **1**, **2**, **3** and **4** are presented in Figure 2. Quantum chemical parameters of **1**, **2**, **3** and **4**, were obtained from calculations, such as energies of the HOMO ( $E_{\text{HOMO}}$ ) and the LUMO ( $E_{\text{LUMO}}$ ), as listed in Table 3. Additional parameters such as HOMO-LUMO energy gap, e.g., absolute electronegativity,  $\chi$ ,



● Carbon atom ● Hydrogen atom ● Nitrogen atom ● Chlorine atom ● Nickel atom

FIGURE 1 Molecular structures with atomic numbering for complexes (1–4)

**TABLE 2** Selected geometric bond lengths and bond angles of complexes

Complex	Bond lengths (Å°)		Bond angles (°)		
[Ni (Cl) <sub>2</sub> (metf)(o-phen)]	Ni(1) - Cl(26)	2.15	Cl(26)-Ni(1)-N(20)	84.03	
	Ni(1) - Cl(25)	2.15	Cl(26)-Ni(1)-N(16)	84.09	
	Ni(1) - N(20)	1.84	Cl(26)-Ni(1)-N(12)	98.16	
	Ni(1) - N(16)	1.83	Cl(26)-Ni(1)-N(2)	98.22	
	Ni(1)- N(12)	1.85	Cl(25)-Ni(1)-N(20)	87.74	
	Ni(1)- N(2)	1.85	Cl(25)-Ni(1)-N(16)	88.01	
			Cl(25)-Ni(1)-N(12)	91.13	
			Cl(25)-Ni(1)-N(2)	91.34	
			N(20)-Ni(1)-N(16)	95.90	
			N(20)-Ni(1)-N(12)	93.65	
			N(16)-Ni(1)-N(2)	93.78	
			N(12)-Ni(1)-N(2)	76.63	
	[Ni (Cl) <sub>2</sub> (metf)(opda)]	Ni(1)-Cl(20)	2.15	Cl(20)-Ni(1)-N(14)	88.42
		Ni(1)-Cl(19)	2.15	Cl(20)-Ni(1)-N(10)	90.41
Ni(1)-N(14)		1.83	Cl(20)-Ni(1)-N(5)	90.36	
Ni(1)-N(10)		1.83	Cl(20)-Ni(1)-N(2)	90.54	
Ni(1)-N(5)		1.83	Cl(19)-Ni(1)-N(14)	90.53	
Ni(1)-N(2)		1.83	Cl(19)-Ni(1)-N(10)	89.08	
			Cl(19)-Ni(1)-N(5)	90.28	
			Cl(19)-Ni(1)-N(2)	90.57	
			N(14)-Ni(1)-N(10)	98.30	
			N(14)-Ni(1)-N(5)	89.68	
			N(10)-Ni(1)-N(2)	89.77	
			N(5)-Ni(1)-N(2)	82.24	
[Ni (Cl) <sub>2</sub> (metf)(en)]		Ni(1)-Cl(16)	2.16	Cl(16)-Ni(1)-Cl(15)	86.66
		Ni(1)-Cl(15)	2.17	Cl(16)-Ni(1)-N(10)	85.27
	Ni(1)-N(10)	1.85	Cl(16)-Ni(1)-N(5)	92.02	
	Ni(1)-N(6)	1.85	Cl(16)-Ni(1)-N(2)	92.23	
	Ni(1)-N(5)	1.38	Cl(15)-Ni(1)-N(10)	78.74	
	Ni(1)-N(2)	1.38	Cl(15)-Ni(1)-N(6)	82.64	
			Cl(15)-Ni(1)-N(2)	84.20	
			N(10)-Ni(1)-N(6)	84.78	
			N(10)-Ni(1)-N(5)	85.61	
			N(6)-Ni(1)-N(5)	96.09	
			N(6)-Ni(1)-N(2)	94.64	
			N(5)-Ni(1)-N(2)	111.43	
	[Ni (Cl) <sub>2</sub> (metf)(2,2'-bipy)]	Ni(1)-Cl(24)	2.15	Cl(24)-Ni(1)-N(18)	86.16
		Ni(1)-Cl(23)	2.15	Cl(24)-Ni(1)-N(14)	84.55
Ni(1)-N(18)		1.83	Cl(24)-Ni(1)-N(10)	91.35	
Ni(1)-N(14)		1.83	Cl(24)-Ni(1)-N(2)	93.04	
Ni(1)-N(10)		1.84	Cl(23)-Ni(1)-N(18)	90.85	
Ni(1)-N(2)		1.84	Cl(23)-Ni(1)-N(14)	88.07	
			Cl(23)-Ni(1)-N(10)	96.21	
			Cl(23)-Ni(1)-N(2)	91.64	
			N(18)-Ni(1)-N(14)	95.47	
			N(18)-Ni(1)-N(10)	87.75	
			N(14)-Ni(1)-N(2)	97.87	
			N(10)-Ni(1)-N(2)	78.78	

chemical potential,  $\pi$ , absolute hardness,  $\eta$ , absolute softness,  $\sigma$ , global electrophilicity,  $\omega$ , global softness, S, and additional electronic charge,  $\Delta N_{\max}$ , were calculated using the following equations:<sup>[45]</sup>

$$E_g = E_{LUMO} - E_{HOMO} \quad (1)$$

$$\chi = -\frac{E_{HOMO} + E_{LUMO}}{2} \quad (2)$$

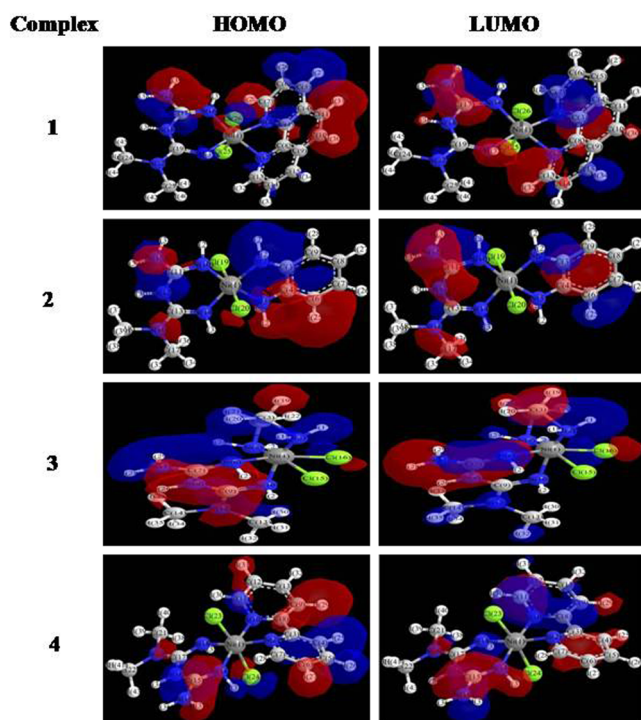


**FIGURE 2** Molecular orbital structures (HOMO and LUMO) for complexes (1–4)

$$\eta = \frac{E_{LUMO} - E_{HOMO}}{2} \quad (3)$$

$$\sigma = \frac{1}{\eta} \quad (4)$$

$$\pi = -\chi \quad (5)$$

$$S = \frac{1}{2\eta} \quad (6)$$

$$\omega = \frac{\pi^2}{2\eta} \quad (7)$$

$$\Delta N_{max} = -\frac{\pi}{\eta} \quad (8)$$

The HOMO and LUMO energy gap is an important stability index. The smaller the value of e.g., the greater is

the reactivity of a compound.<sup>[46]</sup> It was found that complex **1** is more reactive than the other complexes, where the value of  $E_g$  for **1**, **2**, **3** and **4** is 1.57, 1.64, 3.82 and 2.07 eV, respectively.

### 3.3 | Kinetic studies

Thermodynamic activation parameters of decomposition processes of samples, namely activation energy, enthalpy, entropy, and Gibbs free energy change of the decomposition were evaluated graphically in Figure 3 by employing the Coats-Redfern relation for complexes **1**, **2**, **3** and **4**.<sup>[47,48]</sup> Data for kinetic thermal studies were shown in Table 4. The high values of the activation energy illustrated to the thermal stability of the complexes.  $\Delta G$  is positive for reaction for which  $\Delta H$  is positive and  $\Delta S$  is negative. The reaction for which  $\Delta G$  is positive and  $\Delta S$  is negative considered as unfavorable or non-spontaneous reaction. Reactions are classified as either exothermic ( $\Delta H < 0$ ) or endothermic ( $\Delta H > 0$ ) on the basis of whether they give off or absorb heat. Reactions can also be classified as exergonic ( $\Delta G < 0$ ) or endergonic ( $\Delta G > 0$ ) on the basis of whether the free energy of the system decreases or increases during the reaction. The correlation coefficients of the Arrhenius plots of the thermal decomposition steps were lie in the range of 0.914 to 0.998 showing good fit with linear function. It is clear that the thermal decomposition process of complexes **1**, **2**, **3** and **4** are non-spontaneous, i.e., the complexes are thermally stable.

### 3.4 | DNA binding studies

#### 3.4.1 | Absorption spectroscopic studies of DNA-complex interactions

Electronic absorption titration is one of the most useful techniques for DNA binding studies. Nickel complexes in water-buffer mixtures show bands in the region 230–300 nm, are assigned to LMCT transitions. When the DNA concentration is increased, the intensity of charge transfer band is also shifted, due to either hypochromism

**TABLE 3** The calculated quantum chemical parameters of the complexes

Complex	HOMO	LUMO	$E_g$	<b>c</b>	<b>n</b>	<b>s</b>	<b>p</b>	<b>s</b>	<b>w</b>	$DN_{max}$
1	-7.175	-5.597	1.578	6.386	0.789	1.267427	-6.386	0.633714	25.84347	8.093790
2	-7.955	-6.307	1.648	7.131	0.824	1.213592	-7.131	0.606796	30.85629	8.654126
3	-6.283	-2.459	3.824	4.371	1.912	0.523013	-4.371	0.261506	4.996245	2.286088
4	-7.401	-5.326	2.075	6.363	1.037	0.963855	-6.363	0.481928	19.51524	6.133494

**FIGURE 3** Plots of  $\ln[g(\alpha)/T^2]$  vs  $1/T^2$  of  $[\text{Ni}(\text{Cl})_2(\text{metf})(\text{o-phen})]$  for different CR models

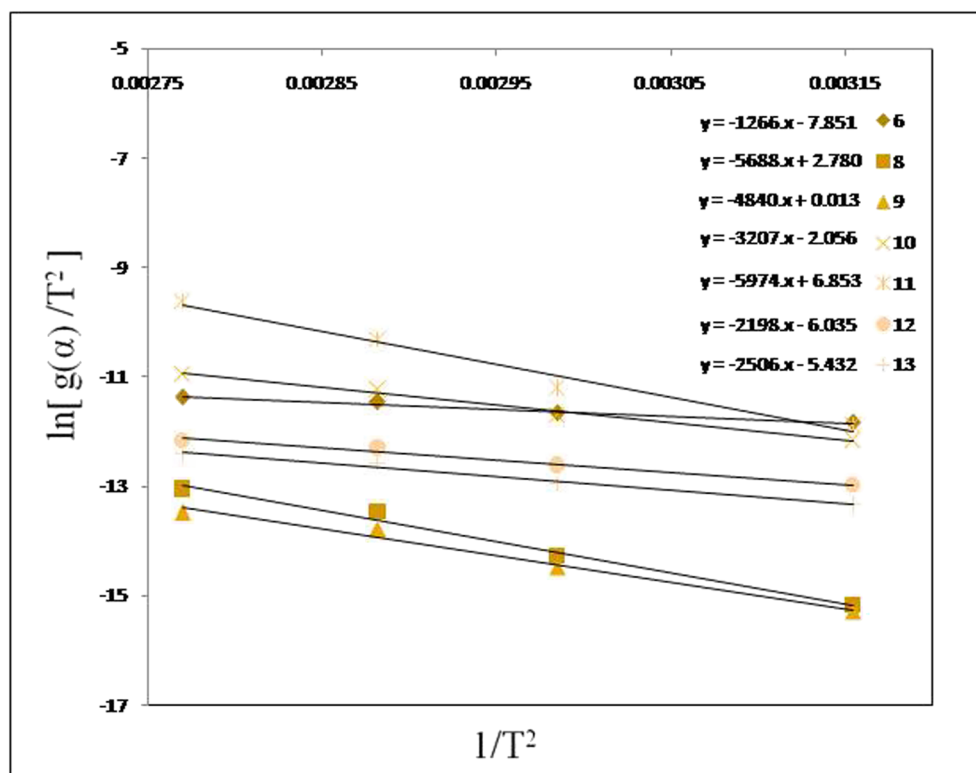


**TABLE 4** Kinetic parameters using Coats- Redfern (CR) method

Complex	Stage	Parameters					
		E (J mole <sup>-1</sup> )	A (S <sup>-1</sup> )	ΔS (J mole <sup>-1</sup> K <sup>-1</sup> )	ΔH (J mole <sup>-1</sup> )	ΔG	r
1	I	4.72 x 10 <sup>4</sup>	9.16x10 <sup>5</sup>	-1.2 x 10 <sup>2</sup>	4.65x 10 <sup>4</sup>	5.71x10 <sup>4</sup>	0.993
2	III	6.06 x 10 <sup>4</sup>	3.45x10 <sup>5</sup>	-1.4 x 10 <sup>2</sup>	5.8 x 10 <sup>4</sup>	9.71x10 <sup>4</sup>	0.998
3	II	8.48 x 10 <sup>4</sup>	2.33x10 <sup>8</sup>	-8.0x 10 <sup>1</sup>	8.33x 10 <sup>4</sup>	9.7 x10 <sup>4</sup>	0.914
4	II	1.05 x 10 <sup>5</sup>	2.81x10 <sup>11</sup>	-2.1 x 10 <sup>1</sup>	1.04x 10 <sup>5</sup>	1.08x10 <sup>5</sup>	0.997

or hyperchromism. The complexes **1**, **2**, **3** and **4** in the presence of DNA show hyperchromism with slight red shift (Figure 4). The complexes can bind to double-stranded DNA in different binding modes on the basis of their structure, charge and type of ligand. As the DNA double helix possesses many hydrogen-bonding sites which are accessible both in minor and major grooves, it is likely that the NH groups of the complexes form hydrogen bonds with N of adenine or O of thymine in DNA, which may contribute to the hyperchromism observed in the absorption spectra.<sup>[49]</sup> The hyperchromic effect may also be due to an electrostatic interaction between positively charged complex and negatively charged phosphate backbone at the periphery of the double helix of CT-DNA.<sup>[50]</sup> Also, a coordination bond of DNA base with Nickel can occur through replacement of the chloride ligand in the complex, probably through aquation as has

been observed with cisplatin.<sup>[51]</sup> From a plot of  $[\text{DNA}]/(\epsilon_a - \epsilon_f)$  versus  $[\text{DNA}]$ ,  $K_b$  is given by the ratio of slope to intercept. The values of  $k_b$  are  $7.42 \times 10^4$ ,  $0.74 \times 10^4$ ,  $3.19 \times 10^4$  and  $5.96 \times 10^4 \text{ M}^{-1}$  for complexes **1**, **2**, **3** and **4** respectively. The intrinsic binding constant ( $K_b$ ) is influenced by planarity of the complex, electron releasing/electron withdrawing groups on ligand and additional Hydrogen bonding.

The difference in the binding constant of the complexes **1**, **2**, **3** and **4** is due to different ancillary ligands. Complex **1** shows more binding strength to double helical DNA than complex **4** due to increased planar aromatic surface area and hydrophobicity of ancillary ligand from bipy to o-phen. Therefore  $K_b$  of complex **1** is greater than complex **4**. The least  $K_b$  value of complex **2** is due to electron releasing group  $\text{NH}_2$  present on opda ligand, may enhance the electron density on complex moiety and

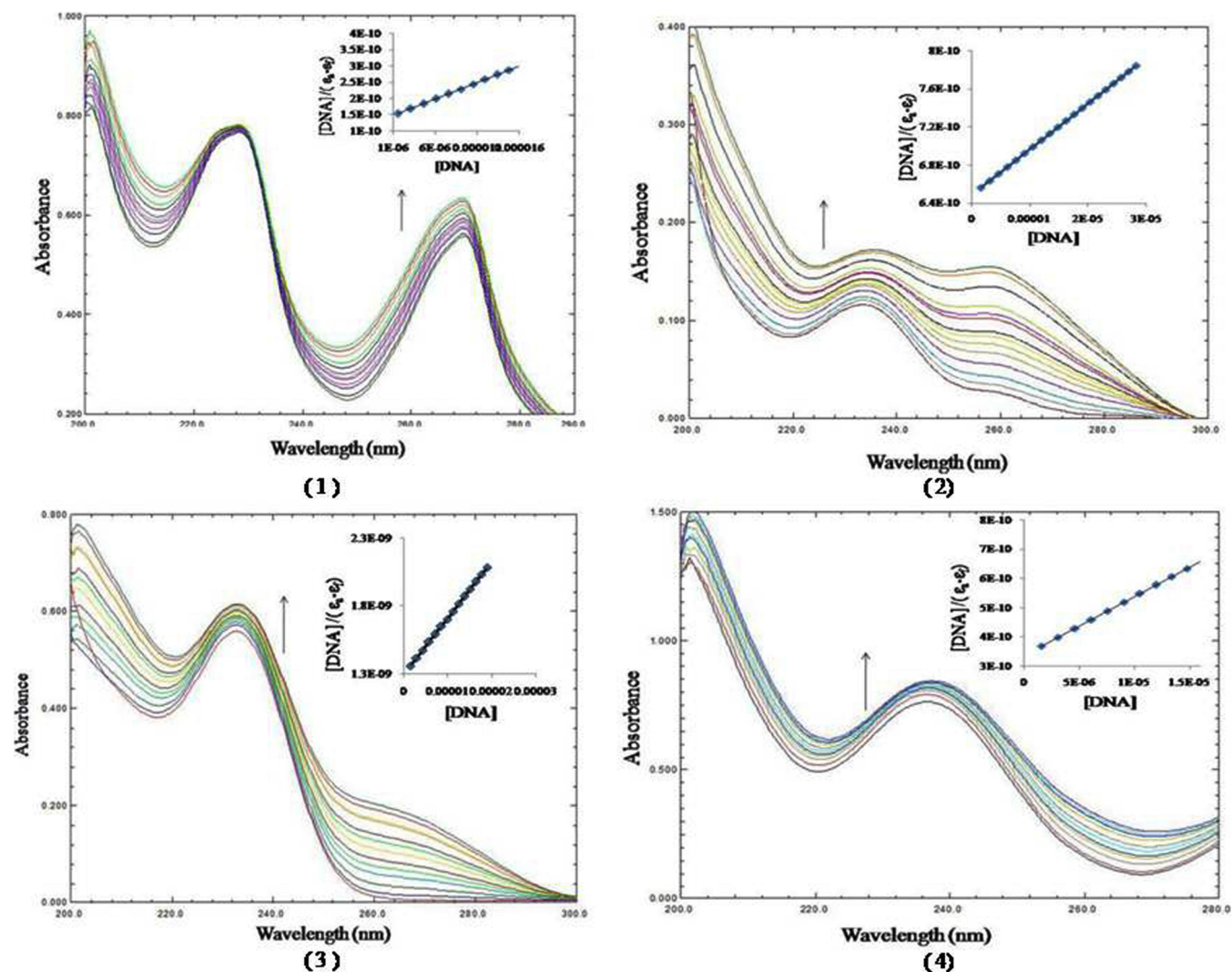


**FIGURE 4** Absorption spectra of 1, 2, 3 and 4 in Tris-HCl buffer upon addition of CT-DNA in absence (lower) and presence (upper) of CT-DNA. ( $[complex] = 20 \mu M$ ;  $[DNA] = 0-100 \mu M$ ). Inset plots of  $DNA/(\epsilon_0 - \epsilon)$  versus  $[DNA]$  for the titration of Ni(II) complexes with DNA. Arrow shows change in absorption with increasing DNA concentrations

makes electron rich. The electron deficient rings interacts more strongly with polyanion (DNA) than electron rich rings. Therefore the electron rich opda ancillary ligand binds less effectively to polyanion (DNA). Likewise the decreasing order of  $K_b$  values of the four complexes i.e. **1** **4** **3** **2** is justified from their chemical structures.<sup>[35,38]</sup> The observed binding constant is more in keeping with groove binding, as reported in the literature.<sup>[10,52-54]</sup> Our results illustrate that the Nickel (II) complexes may bind to DNA via groove binding.

### 3.4.2 | Steady-state emission studies

The emission spectra of the complexes in the presence of DNA allow an investigation of the interaction between

complexes and DNA. The emission intensity of complexes **1**, **2**, **3** and **4** from their LMCT excited states at around 600 nm is found to depend on the DNA concentration. These four complexes in the absence of DNA emit luminescence in Tris-HCl buffer. Upon addition of CT-DNA, the emission intensities increase as shown in Figure 5 This implies that the complexes can strongly interact with DNA and be protected by DNA efficiently. The hydrophobic environment inside the DNA helix reduces the accessibility of solvent water molecules to the duplex and the complex mobility is restricted at the binding site, which leads to a decrease in the vibrational modes of relaxation. To obtain intrinsic binding constants, fluorescence data were cast into a modified Scatchard equation<sup>[27]</sup> through a plot of  $r/C_f$  versus  $r$ , where  $r$  is the binding ratio of  $C_b/[DNA]$  and  $C_f$  is the free ligand

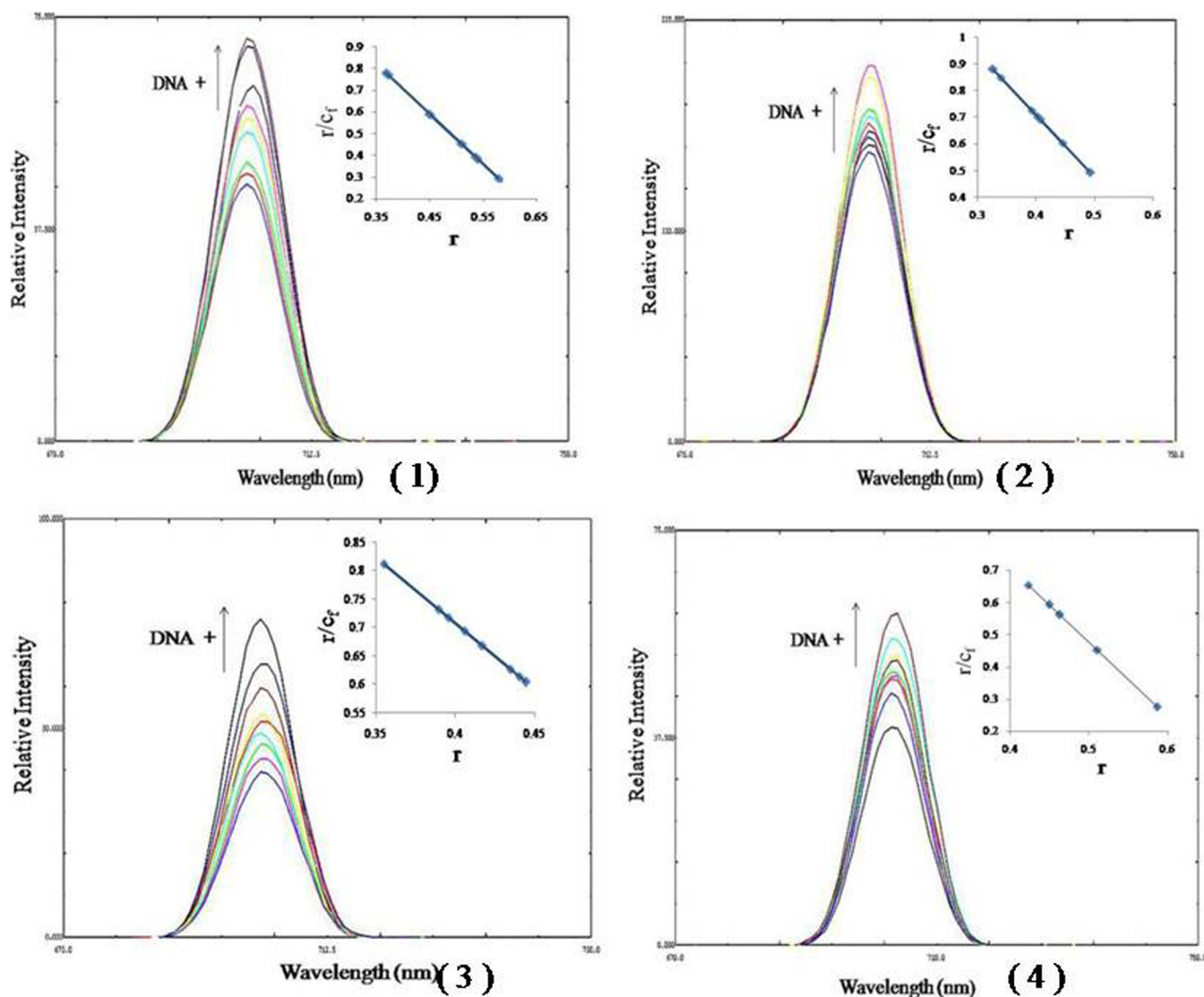


**FIGURE 5** Emission spectra of 1, 2, 3 and 4 in Tris-HCl buffer at 25 °C upon addition of CT-DNA, ( $[\text{Complex}] = 10 \mu\text{M}$ ;  $[\text{DNA}] = 10\text{--}200 \mu\text{M}$ ). The arrow shows the increase in intensity upon increasing CT-DNA concentrations

concentration. The binding constants ( $K_b$ ) are  $2.51 \times 10^4$ ,  $2.17 \times 10^4$ ,  $2.24 \times 10^4$  and  $2.32 \times 10^4 \text{ M}^{-1}$  for complexes **1**, **2**, **3** and **4** respectively. The calculated binding constants are also comparable with UV absorption data. The binding constants obtained from luminescence titration are different from those obtained from absorption studies.<sup>[55]</sup> This small difference between the two sets of binding constants is due to the different spectroscopic techniques and different calculation methods; however, they are comparable.

### 3.4.3 | Quenching studies

Fluorescence quenching experiments were performed to obtain an estimate of the relative binding affinity of

the complexes to CT-DNA with respect to EB. It is well-known that free EB displays a decrease in emission intensity in Tris-HCl buffer medium because of quenching by solvent molecules. However EB strongly fluoresces in the presence of DNA due to complete intercalation between adjacent DNA base pairs, a process that can be reversed by the addition of a competing agent. The quenching curves of EB bound to DNA in the absence and presence of **1**, **2**, **3** and **4** are shown in Figure 6. The addition of the complexes to DNA pre-treated with EB causes appreciable reduction in the emission intensity. This result is also in favor of groove binding of the complexes to CT-DNA.<sup>[56]</sup> These data were analyzed by means of Stern-Volmer equation. The quenching plots (insets of Figure 6) illustrate that the fluorescence quenching of EB bound to DNA by **1**,

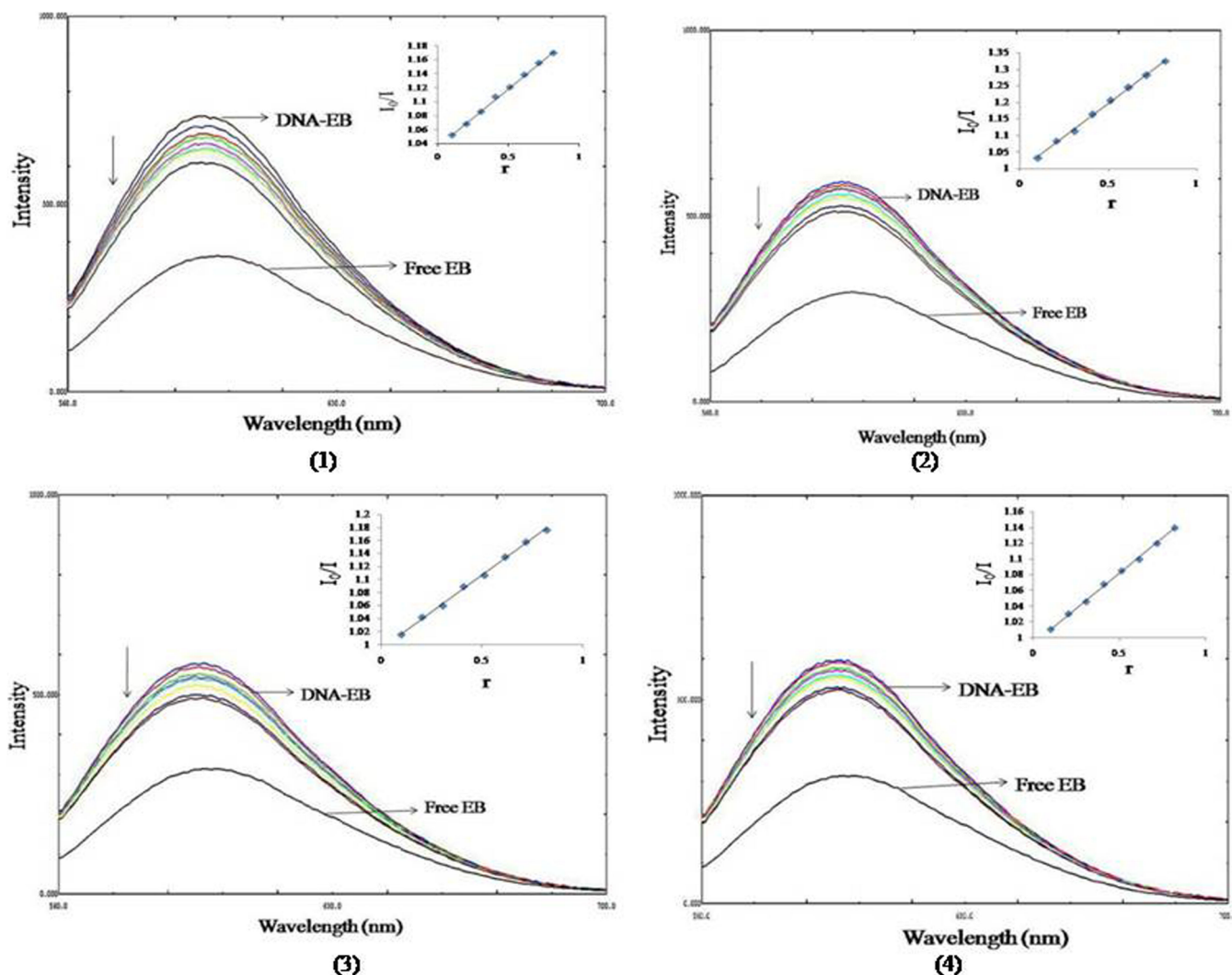


**FIGURE 6** Emission spectra of EB bound to CT-DNA in the absence and presence of complexes (1-4) ([Complex] = 0-100  $\mu\text{M}$ , [DNA] = 130  $\mu\text{M}$ , [EB] = 40  $\mu\text{M}$ ). Insets: Stern-Volmer quenching curves

2, 3 and 4 is in linear agreement with the Stern-Volmer relationship, which corroborates that the complexes bind to DNA. From a plot of  $I_0/I$  versus  $[\text{complex}]/[\text{DNA}]$ ,  $K_{\text{sq}}$  is given by the ratio of slope to intercept. The  $K_{\text{sq}}$  values for 1, 2, 3 and 4 are 0.16, 0.40, 0.23 and 0.18 respectively. To quantify the displacement, the concentration of the complex at which EB fluorescence decreases by 50% (assumed to be 50% displacement of EB) is calculated, from a plot of  $I/I_0$  vs  $[\text{complex}]$  using regression analysis (Figure 7). The apparent DNA binding constant values for 1, 2, 3 and 4 were calculated from a competitive binding model with equation,  $K_{\text{app}} = K_{\text{EB}} \times [\text{EB}]_{50\%} / [\text{complex}]_{50\%}$ , where  $K_{\text{app}}$  is the apparent DNA binding constant of the complex,  $K_{\text{EB}}$  is the binding constant of EB i.e.  $1.25 \times 10^6 \text{ M}^{-1}$ ,  $[\text{EB}]_{50\%}$  and  $[\text{complex}]_{50\%}$  are the concentrations of EB and complex at 50% fluorescence.  $K_{\text{app}}$  values for 1, 2,

3 and 4 are  $1.19 \times 10^5$ ,  $2.38 \times 10^5$ ,  $1.45 \times 10^5$ ,  $1.12 \times 10^5 \text{ M}^{-1}$ .

### 3.4.4 | Light switch studies

Light switch studies were conducted using a literature method.<sup>[57]</sup> As shown in Figure 8, upon addition of DNA to complexes 1, 2, 3 and 4, its emission intensity is increased (light switch on). This is because the complexes bind to DNA to form DNA-[Ni (II)complex]. The emission of bound complex is quenched by cobalt (II) ion, thus turning the light switch off,<sup>[58,59]</sup> due to formation of heterometallic complex  $\text{Co}^{+2}$ -[Ni (II) complex]. When EDTA is added into the buffer system containing heterometallic complex, emission intensity is recovered (switch on) again. This is due to the formation of  $[\text{Co}^{+2}$ -

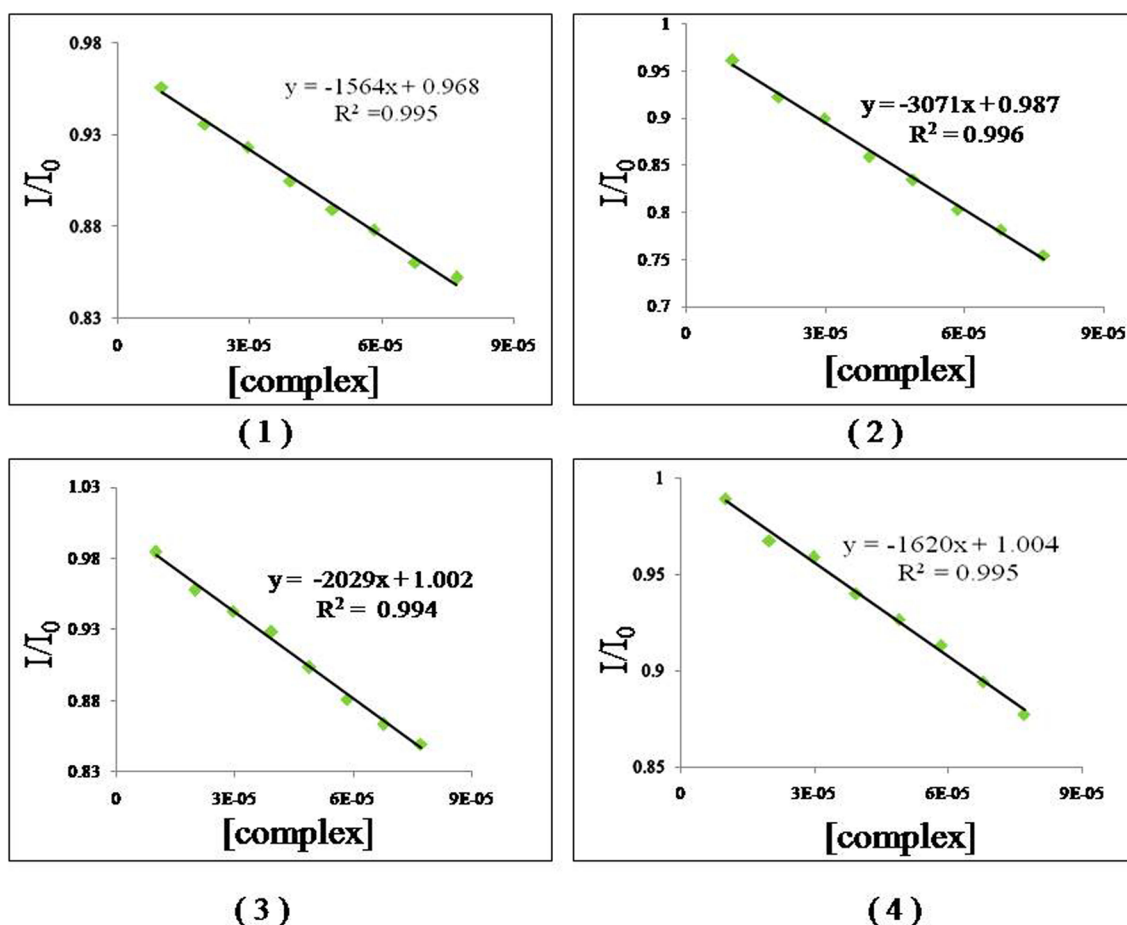


**FIGURE 7** Competitive DNA binding- Kapp plots of complexes 1, 2, 3 and 4

EDTA] complex and free Nickel (II) complex (**1**, **2**, **3** and **4**) again interacts with DNA. The change in the luminescence of the DNA-bound complex in the presence of  $\text{Co}^{+2}$  and EDTA reveals a potential in the modulation of drug therapy.

### 3.4.5 | Viscosity studies

A classical intercalation model demands that the DNA helix must lengthen as base pairs are separated to accommodate a binding ligand, leading to an increase in DNA viscosity.<sup>[60]</sup> In contrast, a partial and/or non-classical intercalation ligand could bend (or kink) the DNA helix, reducing its effective length and concomitantly reducing its viscosity, while ligands that bind exclusively in DNA grooves (e.g. netropsin, distamycin), under the same conditions, typically cause less pronounced changes (positive or negative) or no changes in DNA solution viscosity.<sup>[61]</sup> The slow increase in relative viscosity of CT-DNA with increasing amount of **1**, **2**, **3** and **4** (Figure 9) indicates groove binding.<sup>[62]</sup> In principle, this could be explained

by changes in conformation, flexibility or solvation of the DNA molecule. This behavior is similar to that of metformin-DNA binding studies reported by Shahabadi and Heidari.<sup>[11]</sup>

### 3.4.6 | Photo-cleavage studies

Many Nickel (II) complexes can cleave DNA under irradiation by UV or visible light. When circular plasmid DNA is subjected to electrophoresis, relatively fast migration will be observed in the intact supercoiled form (Form I). When scission occurs on one strand (nicked), the supercoil relaxes to generate a slower-moving open circular form (Form II). Finally, when both strands are cleaved, a linear form (Form III) is obtained, which migrates at a speed between those of Forms I and Form II.<sup>[63]</sup> Figure 10 shows the extent of DNA photo-cleavage at four different concentrations (10  $\mu\text{l}$ , 20  $\mu\text{l}$ , 30  $\mu\text{l}$ , 40  $\mu\text{l}$ ) of the complexes **1**, **2**, **3** and **4** at 360 nm for 1 hr. No DNA cleavage is observed in controls in which complex is absent. All

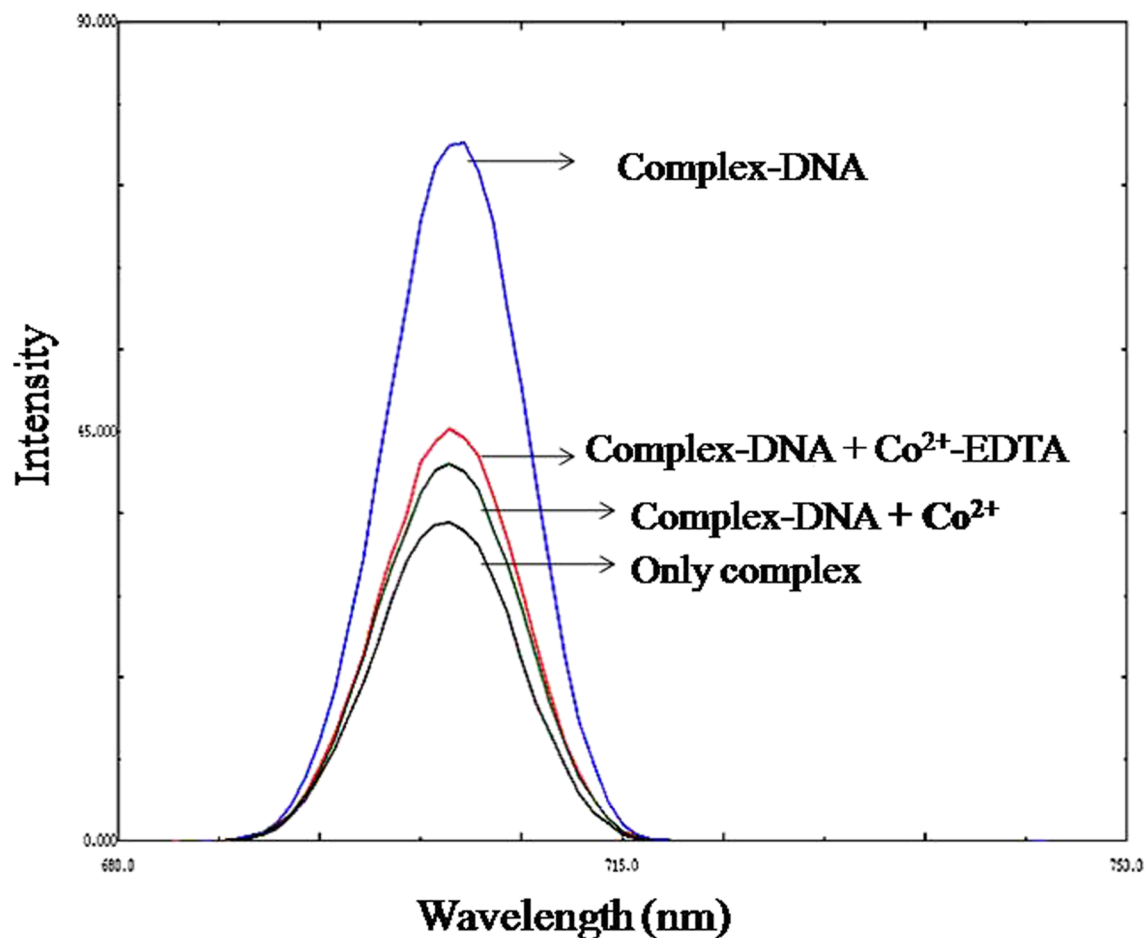


**FIGURE 8** DNA light switch on and off experiments showing the luminescence changes upon addition of  $\text{Co}^{2+}$ , EDTA to  $[\text{Ni}(\text{Cl})_2(\text{metf})(\text{o-phen})] + \text{DNA}$

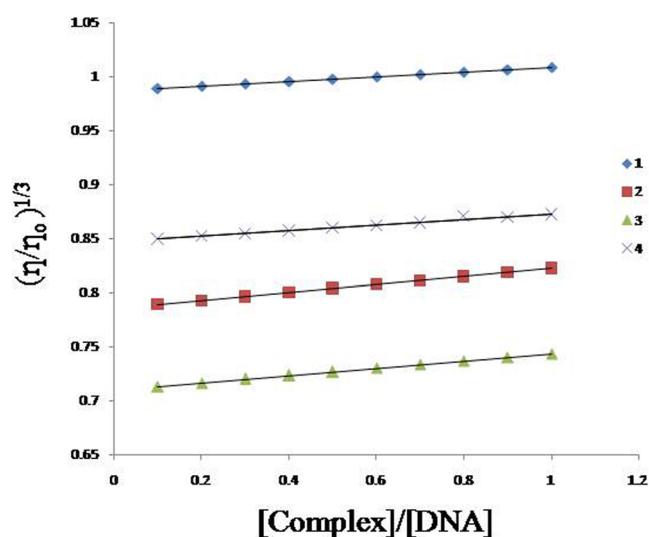


**FIGURE 9** Effect of increasing amount of complexes 1, 2, 3 and 4 on the relative viscosities of CT-DNA at room temperature in 5 mM Tris-HCl buffer. The total concentration of DNA = 20  $\mu\text{M}$ ,  $[\text{complex}] = 0\text{--}100 \mu\text{M}$

the four complexes exhibit DNA photocleavage activity, with the increasing concentration of complexes (1, 2, 3 and 4) the amount of form I is decreased whereas that of form II is increased. The cleavage effect was found to be concentration dependent. Among all the four complexes, complex 1 exhibits higher efficiency of DNA cleavage than other three complexes. The role of Oxidant  $\text{H}_2\text{O}_2$  is to oxidise metal complex and releases OH free radical. This OH free radical participates in the oxidation of the deoxyribose moiety, followed by hydrolytic cleavage of sugar phosphate backbone.<sup>[64]</sup> The delivery of high concentration of metal ion to the helix, in locally generating oxygen or hydroxide radicals lead to an efficient DNA cleavage reaction.

### 3.5 | In Silico molecular docking study

Discovery Studio 2.1 software was used to perform docking between the metal complex. (ligand) and B-DNA

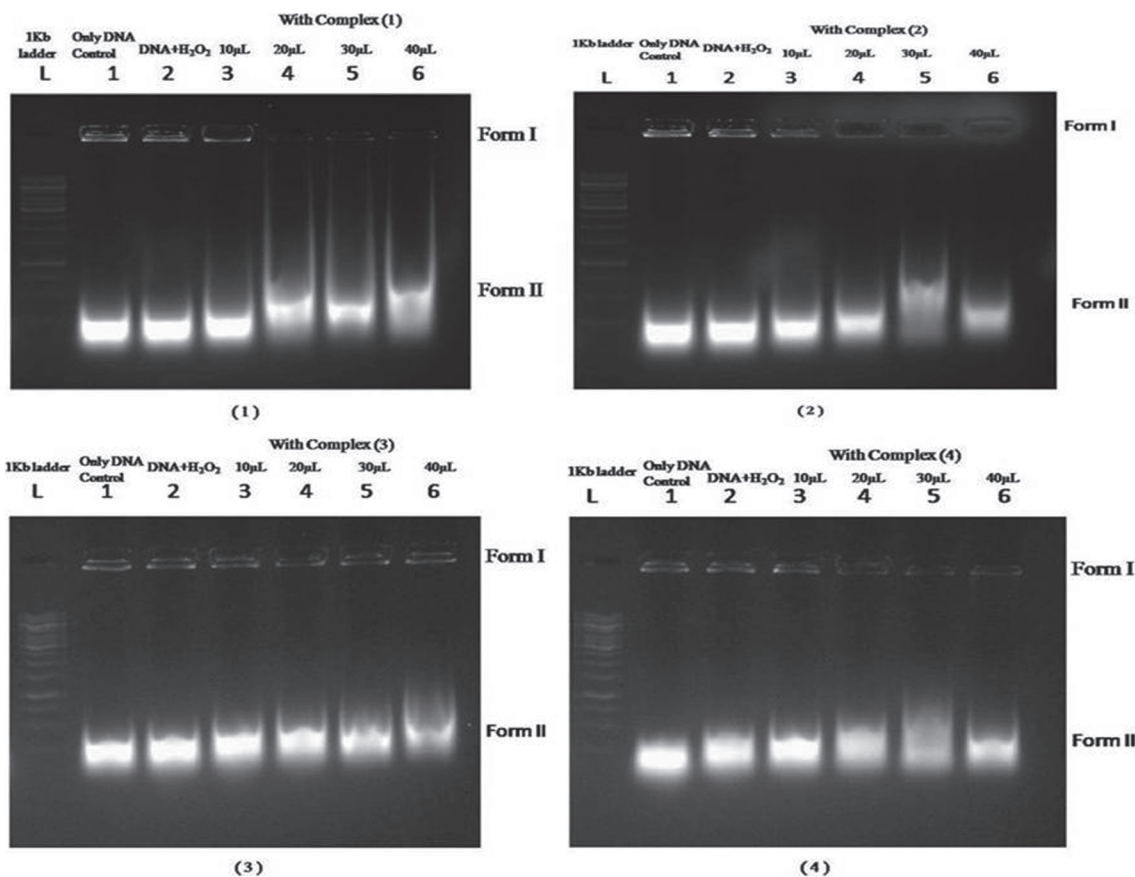


**FIGURE 10** Changes in the Agarose gel electrophoresis pattern by oxidative cleavage of supercoiled pUC19 plasmid DNA, induced by H<sub>2</sub>O<sub>2</sub> in the absence and presence of metal complexes 1, 2, 3 and 4 at four different concentrations of 10 μl, 20 μl, 30 μl, 40 μl after 60 min irradiation at 360nm

**TABLE 5** Docking energy and ligand interaction data of the compound

Complex	CDocker Intectraction energy	Interacting atoms	H-Bond Distance (Å°)	Donor	Acceptor	No. of H-bonds
1	32.027	ophen: H34 - B:DC18:O4'	2.265000	H34	O4'	2
		ophen: H35 - B:DG19:O4'	1.939000	H35	O4'	
		ophen: H34 - B:DC18:H4'	1.677000	H34	H4'	
2	31.427	opda: H20 - B:DG19:O4'	1.988000	H20	O4'	2
		opda: H26 - B:DA17:N3	2.437000	H26	N3	
3	35.393	en: H22 - B:DC18:O4'	2.413000	H22	O4'	4
		en: H21 - B:DG19:O4'	2.216000	H21	O4'	
		en: H20 - A:DC9:O4'	2.380000	H20	O4'	
		en: H23 - B:DG19:O4'	1.839000	H23	O4'	
		A:DC9:H4' - en: H20	1.751000	H4'	H20	
4	30.521	bipy: H32 - B:DG19:O4'	1.917000	H32	O4'	2
		bipy: H33 - B:DC18:O4'	2.174000	H33	O4'	
		B:DC18:H1' - bipy: H33	1.806000	H1'	H33	

(Continues)

TABLE 5 (Continued)

Complex	CDocker Intectraction energy	Interacting atoms	H-Bond Distance (A°)	Donor	Acceptor	No. of H-bonds
Metformin	37.561	A:DG7:H21 - Met:N3	2.472000	H21	N3	4
		Met:H16 - B:DG19:O4'	2.408000	H16	O4'	
		Met:H19 - B:DC18:O2	2.127000	H19	O2	
		Met:H20 - B:DC18:O4'	2.078000	H20	O4'	

(receptor) sequence. Input used for the docking is B-DNA sequence 5'-D(\*AP \* CP \* CP \* GP \* AP \* CP \* GP \* TP \* CP \* GP \* GP \* T)-3' retrieved from protein data bank (PDB ID: 423D) at a resolution of 1.6 Å and the 3D models of the metal complexes. Receptor was prepared by deleting all the heteroatoms including water and by adding polar hydrogen atoms, docking energy (CDocker Intectraction energy) of title derivatives were explored towards target. From the docking analysis of B-DNA sequence with the synthesized complexes, unveiled their

docking scores and interaction patterns. The docked complexes 1, 2, 3 and 4 exhibited fitness scores with a range of 35.393 to 30.521 as compared to metformin 37.561 (Table 5). Among all the compounds, Compound 3 was ranked highest docking score of 35.393. These results indicate that both the compounds bound within the binding site pocket of metformin similar binding pattern with one of the binding site (DG19) nucleotide residue. The protein–ligand interaction visualization of the compounds is shown in Figure 11.

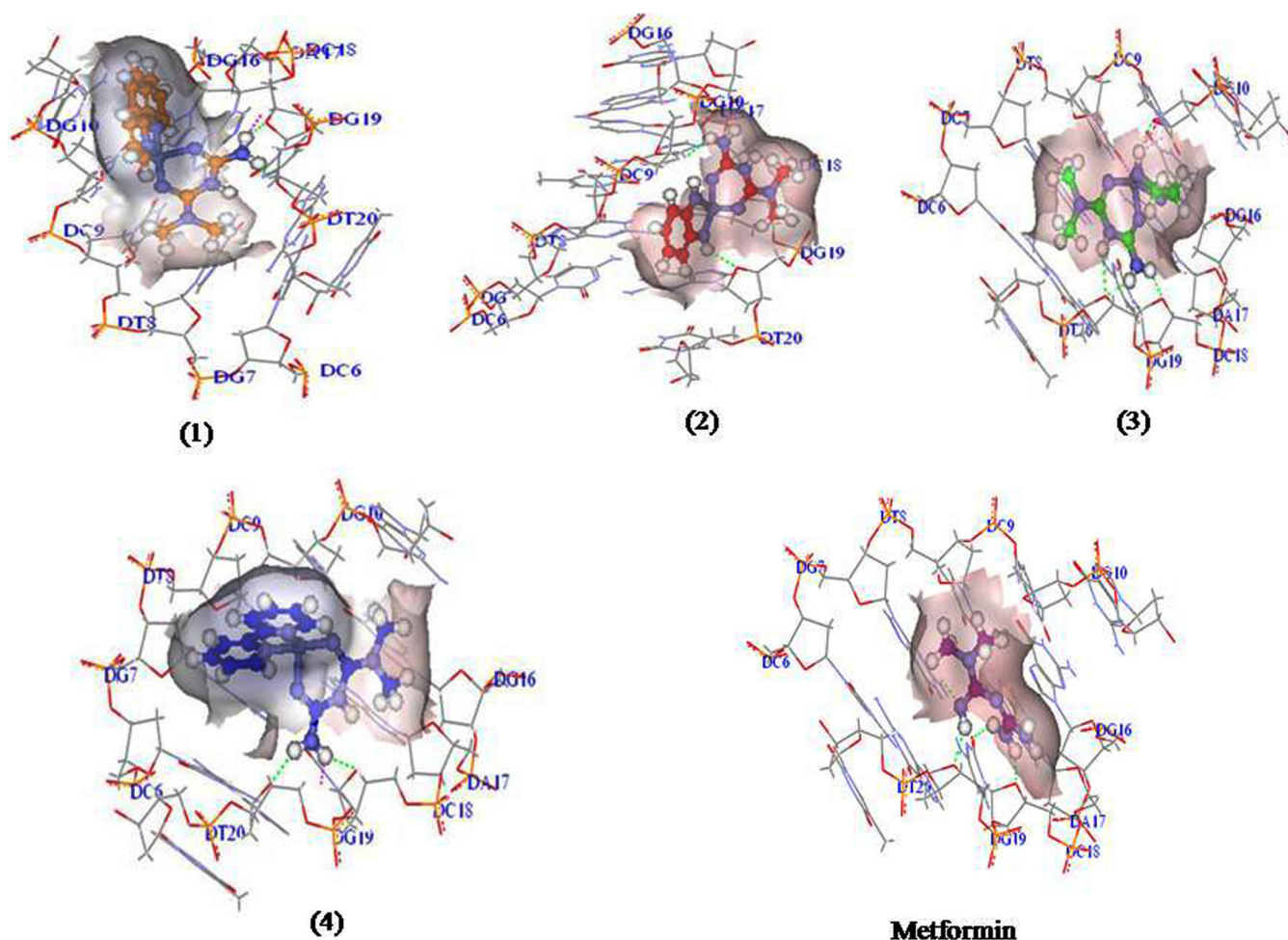


FIGURE 11 Receptor-ligand hydrogen bonds (green colour) and bumps (pink colour) of complexes (1-4) and Metformin with B-DNA sequence (PDB : 423D)

## 4 | CONCLUSIONS

Four new Ni (II) ternary complexes of metformin were synthesized and the structure of these complexes were proposed based on the analytical, conductance, thermal, spectral and magnetic moment data. Finally, octahedral geometry has been suggested for all four complexes. The non-electrolytic nature of these complexes was confirmed on the basis of their molar conductance values. Elemental analysis shows the ratio of metformin, auxiliary ligand, Nickel (II) in the complexes as 1:1:1. The stability of all the complexes was discussed and kinetic parameters ( $E^*$ ,  $A$ ,  $\Delta H^*$ ,  $\Delta S^*$  and  $\Delta G^*$ ) of all thermal decomposition stages have been estimated using the Coats–Redfern method. From the kinetic studies it is clear that the thermal decomposition process of these complexes are non-spontaneous, i.e. the complexes are thermally stable. Geometrical optimized structures of these complexes is given by optimizing their bond lengths, bond angles and torsional angles. The experimental results of DNA binding studies suggest that complexes **1**, **2**, **3** and **4** bind to DNA via groove binding with activity in the order **1** **4** **3** **2**. The Fluorescence quenching studies gives  $K_{sq}$  values for **1**, **2**, **3** and **4** are 0.16, 0.40, 0.23 and 0.18 respectively. The molecular docking technique was employed to determine the binding affinity of the complexes with DNA and protein molecules. Complex **3** was ranked with highest docking score of 35.393. Nuclease studies showed that, upon irradiation these complexes show effective cleavage of pUC19DNA using  $H_2O_2$  as an oxidant.

## ACKNOWLEDGMENTS

The authors thank OU-DST-PURSE-II programme for providing financial assistance to carry out this work.

## REFERENCES

- [1] P. Zhao, S. Zhai, J. Dong, L. Gao, X. Liu, L. Wang, J. Kong, L. Li, *Bioinorg. Chem. Appl.* **2018**, 8478152.
- [2] H. Liu, L. Li, Q. Guo, J. Dong, J. Li, *Transition Met. Chem.* **2013**, 38, 441.
- [3] L. Li, Q. Guo, J. Dong, T. Xu, J. Li, *J. Photochem. Photobiol. B* **2013**, 125, 56.
- [4] S. Tabassum, M. Ahmad, M. Afzal, M. Zaki, P. K. Bharadwaj, *J. Photochem. Photobiol. B* **2014**, 140, 321.
- [5] B. Hwa-Yun, S. Hee-Jeon, T. S. Cho, Y. S. Yoon, U. Sehlstedt, S. K. Kim, *Biophys. Chem.* **1998**, 70, 1.
- [6] J. H. Tan, Y. J. Lu, Z. S. Huang, L. Q. Gu, J. Y. Wu, *Eur. J. Med. Chem.* **2007**, 42, 1169.
- [7] S. S. Sharma, J. V. Ramani, D. P. Dalwadi, J. J. Bhalodia, N. K. Patel, D. D. Patel, R. K. Patel, *Eur. J. Chem.* **2011**, 8, 361.
- [8] P. Hubberstey, U. Suksangpanya, *Struct. Bonding* **2004**, 111, 33.
- [9] R. Olar, A. Dogaru, D. Marinescu, M. Badea, *J. Therm. Anal. Calorim.* **2012**, 110, 257.
- [10] R. Olar, M. Badea, E. Cristurean, C. Parnau, D. Marinescu, *J. Therm. Anal. Calorim.* **2006**, 1, 53.
- [11] N. Shahabadi, L. Heidari, *Spectrochim. Acta A* **2012**, 97, 406.
- [12] N. Shahabadi, L. Heidari, *Spectrochim. Acta A* **2014**, 128, 377.
- [13] M. Can, Armstrong, S. W. Ragsdale, *Chem. Rev.* **2014**, 114, 4149.
- [14] M. Alexion, I. Tsivikas, C. Dendrinou-Samara, A. A. Pantazaki, P. Trikalitis, N. Lalioti, D. A. Kyriakidis, D. P. Kessissoglou, *J. Inorg. Biochem.* **2003**, 93, 256.
- [15] R. del Campo, J. J. Criado, E. Garcia, et al., *J. Inorg. Biochem.* **2002**, 89, 74.
- [16] M. Tasmina Khatun, M. Abdul Alim, M. Kudrat-E-Zahan, M. M. Alam, N. Uddin, M. M. Haque, M. Y. Reza, *Adv Appl. Sci. Res.* **2016**, 7, 49.
- [17] Y. Harinath, D. Subba Rao, C. Suresh, K. Seshaiiah, *J. Chem. Sci.* **2016**, 128, 43.
- [18] K. Mancha Madha, N. Ramalakshmi, *J. Adv. Che. Sci.* **2017**, 3, 469.
- [19] E. Jabri, M. B. Carr, R. P. Hausinger, P. Karplus, *Science* **1995**, 268, 998.
- [20] N. Selvakumaran, N. S. P. Bhuvanesh, A. Endo, R. Karvembu, *Polyhedron* **2014**, 75, 95.
- [21] A. E. M. Ramadan, *J. Mol. Struct.* **2012**, 1015, 56.
- [22] J. Marmur, *J. Mol. Biol.* **1961**, 3, 208.
- [23] M. E. Reichmann, S. A. Rice, C. A. Thomas, P. Doty, *J. Am. Chem. Soc.* **1954**, 76, 3047.
- [24] B. N. Figgis, J. Lewis, R. C. Wilkinson (Eds), *Wiley Interscience*, New York **1967**.
- [25] A. Wolfe, G. H. Shimer, T. Meehan, *Biochemistry* **1987**, 26, 6392.
- [26] K. S. Ghosh, B. K. Sahoo, D. Jana, S. Dasgupta, *J. Inorg. Biochem.* **2008**, 102, 1711.
- [27] A. Srishailam, Y. Praveen Kumar, P. Venkat Reddy, N. Navaneetha, V. Uma, S. Surya Singh, S. Satyanarayana, *J. Photochem. Photobiol. B* **2014**, 132, 111.
- [28] S. Satyanarayana, J. C. Dabrowiak, J. B. Chaires, *Biochemistry* **1992**, 31, 9319.
- [29] L. K. Gupta, S. Chandra, *Spectrochim. Acta A* **2006**, 65, 792.
- [30] D. Inci, R. Aydm, O. Vatan, T. Sevgi, D. Yilmaz, Y. Zorlu, Y. Yerli, B. Cosut, E. Demirkan, N. Cilkilic, *J. Biol. Inorg. Chem.* **2017**, 22, 61.
- [31] K. Nakamoto, *Infrared and Raman Spectra of Inorganic and co-ordination compounds*, third ed., John Wiley & Sons, New York **1978** p. 228.
- [32] R. Olar, M. Badea, E. Cristurean, V. Lazar, R. Cernat, C. Balotescu, *J. Therm. Anal. Calorim.* **2005**, 80, 451.
- [33] N. Koteswara Rao, M. M. Annapurna, *JASA* **2007**, 3, 43.
- [34] G. Patrinoiu, L. Patron, O. Carp, N. Stanica, *J. Therm. Anal. Calorim.* **2003**, 72, 489.
- [35] P. Rabindra Reddy, S. Rajeshwar, B. Satyanarayana, *J. Photochem. Photobiol. B* **2016**, 1600, 217.
- [36] P. Vasantha, B. Sathish Kumar, B. Shekar, P. V. Anantha, *Appl. Organomet. Chem* **2018**, 32, e4074.
- [37] P. Pallavi, P. Nagababu, J. N. L. Latha, S. Satyanarayana, *Helv. Chem. Acta* **2007**, 90, 627.
- [38] P. R. Reddy, N. Raju, P. Manjula, K. V. G. Reddy, *Chem. Bio-divers.* **2007**, 4, 1565.
- [39] R. B. Xiu, F. L. Mintz, X. Z. You, R. X. Wang, Q. Yue, Q. J. Meng, Y. J. Lu, D. V. Derveer, *Polyhedron* **1996**, 15, 4585.

- [40] P. Ponya Ulthra, N. Pravin, N. Raman, *J. Photochem. Photobiol. B* **2016**, *158*, 136.
- [41] F. A. Cotton, G. Wilkinson, *Advanced Inorganic Chemistry*, Fifth ed., Wiley, New York **1988**.
- [42] V. Muniyandi, N. Pravin, P. Subbaraj, N. Raman, *J. Photochem. Photobiol. B* **2016**, *156*, 11.
- [43] S. G. Shirodkar, P. S. Mane, T. K. Chondhekar, *Indian J. Chem.* **2001**, *40*, 1114.
- [44] B. N. Figgs, Wiley, New York **1966**.
- [45] B. Shekar, P. Vasantha, B. Sathish Kumar, P. V. Anantha Lakshmi, *Appl. Organomet. Chem.* **2018**, *32*, e4254.
- [46] A. Z. El-Sonbati, M. A. Diab, A. A. El-Bindary, M. I. Abou-Dobara, H. A. Seyam, *J. Mol. Liq.* **2016**, *218*, 434.
- [47] A. W. Coats, J. P. Redfern, *Nature* **1964**, *201*, 68.
- [48] M. S. Refat, H. M. A. Al-Maydama, F. Al-Azab, R. Amin, Y. M. S. Jamil, *Spectrochim. Acta A* **2014**, *128*, 427.
- [49] H. Chao, W. -J. Mei, Q. -W. Huang, *J. Inorg. Biochem.* **2002**, *92*, 165.
- [50] Y. N. Xiao, C. X. Zhan, *J. Appl. Polym. Sci.* **2002**, *84*, 887.
- [51] S. E. Sherman, D. Gibson, A. H. J. Wang, S. J. Lippard, *J. Am. Chem. Soc.* **1988**, *110*, 7368.
- [52] F. Arjmand, F. Sayeed, *J. Mol. Struct.* **2010**, *965*, 14.
- [53] S. Sharma, S. Singh, K. M. Chandra, D. S. Pandey, *J. Inorg. Biochem.* **2005**, *99*, 458.
- [54] Q. L. Zhang, J. G. Liu, J. Liu, G. Q. Xue, *J. Inorg. Biochem.* **2001**, *85*, 291.
- [55] J. B. Chaires, N. Dattagupta, D. M. Crothers, *Biochemistry* **1982**, *21*, 3927.
- [56] J. E. N. Dolatabadi, V. PanahiAzar, A. Barzegar, A. A. Jamali, F. Kheirdoosh, S. Kashanian, Y. Omid, *RSC Adv.* **2014**, *4*, 64559.
- [57] N. Deepika, Y. Praveen Kumar, C. S. Devi, P. V. Reddy, A. Srishailam, S. Satyanarayana, *J. Biol. Inorg. Chem.* **2013**, *18*, 751.
- [58] Y. Liu, A. Chouai, N. N. Degtyareva, D. A. Lutterman, K. R. Dunbar, C. Turro, *J. Am. Chem. Soc.* **2005**, *127*, 10796.
- [59] M. Chen, H. Li, Q. Li, Z. Xu, *Spectrochim. Acta A Mol. Biomol. Spectrosc.* **2010**, *75*, 1566.
- [60] M. B. Gholivand, S. Kashanian, H. Peyman, H. Roshanfekr, *Eur. J. Med. Chem.* **2011**, *46*, 2630.
- [61] F. Arjmand, M. Aziz, *Eur. J. Med. Chem.* **2009**, *44*, 834.
- [62] P. X. Xi, Z. Xu, X. H. Liu, F. J. Chen, Z. Z. Zeng, X. W. Zhang, Y. Liu, *J. Fluoresc.* **2009**, *19*, 63.
- [63] P. R. Reddy, P. Manjula, *Chem. Biodivers.* **2007**, *4*, 468.
- [64] N. Raman, R. Jeyamurugan, R. S. Kumar, B. Raj Kapoor, S. G. Franzblau, *Eur. J. Med. Chem.* **2010**, *45*, 5438.

**How to cite this article:** Rajeshwari K, Vasantha P, Kumar BS, Shekhar B, Lakshmi PVA. Water Soluble Nickel – metformin ternary complexes: Thermal, DNA binding and molecular docking studies. *Appl Organometal Chem.* 2019; e5351. <https://doi.org/10.1002/aoc.5351>